Journal of Research and Applications in Mechanical Engineering
ISSN: 2229-2152 (Print); 2697-424x (Online)
(2026) Vol. 14, No. 1, Paper No. JRAME 26-14-010
[DOI: 10.14456/ jrame.2026.10]

Research Article

Impact of Biaxial Loading on the Buckling Delamination Mode of the Pzt+Metal+Pzt Sandwich Rectangular Thick Plate With Embedded Interface Cracks

F. Aylikci
U.B. Yesil*
Department of Mathematical Engineering, Faculty of Chemical and Metallurgical Engineering, Yildiz Technical University, Istanbul, 34220, Turkey

Received 5 December 2024
Revised 28 February 2025
Accepted 3 April 2025

Abstract:
This research investigates the buckling delamination mode of embedded interface cracks in a PZT+Metal+PZT sandwich plate, utilizing the piecewise homogenous body model and the three-dimensional linearized theory of stability loss for piezoelectric materials. An interface rectangular crack is presumed to exist between the layers of the face and the core, with the plate subjected to bi-axial uniformly distributed compressive forces acting on the vertical sides of the rectangular sandwich plate. The surfaces of the analyzed interface cracks are presumed to possess negligible initial defects prior to loading, and the progression of these initial imperfections under bi-axial compressive forces is examined. Based on the initial imperfection criterion, the critical buckling pressures for local delamination caused by buckling of the rectangular plate around cracks are determined [1]. When the loading levels are beneath the critical threshold, the crack edges display surface wrinkles. This study seeks to examine and evaluate surface wrinkles about diverse geometric and material aspects.

Keywords: *PZT sandwich thick plate, Surface wrinkles, Buckling delamination, Embedded crack, Critical force, 3D FEM*

1. Introduction

The buckling delamination of plates with cracks or defects is a critical area of study in structural mechanics [1]. Research has explored various aspects, including sandwich plates [2], viscoelastic sandwich plates with interface cracks [3], thick sandwich plates with through-width delamination [4], composite plates with pre-existing circular delamination [5], and debonded sandwich panels with soft cores [6]. These studies employ different analytical approaches, such as three-dimensional geometrically nonlinear field equations, shear deformation plate theories, finite element methods, and variational principles. Factors influencing buckling behavior include material properties, crack location and geometry, loading conditions, and boundary conditions. The research highlights the importance of considering multiple failure modes, as the dominant mode may change during delamination progression. Additionally, higher-order theories have been found to provide more accurate results compared to first-order models in predicting mechanical fields and critical loads.

Local buckling delamination in piezoelectric-metal layered composites may occur due to the presence of debonded regions between the layers when subjected to compression. The occurrence of local buckling delamination is more prevalent in the piezoelectric layers adhered to the surface of a host structure composed of elastic materials, such as metals.

* Corresponding author: U.B. Yesil
E-mail address: ubabuscu@yildiz.edu.tr

The agglutination procedure occurs when piezoelectric plates are affixed to structures and utilized like receivers or detectors during different forms of non-destructive testing for defects [7]. Delaminated piezoelectric elastoplastic laminated beams subjected to hygrothermal conditions were studied for postbuckling and delamination growth in [8]. These assembly processes result in the rupture of the bonds formed at the surface between the elastic and piezoelectric substrates, causing local buckling and delamination of the substrates under compression. To reduce buckling delamination, electromechanical relationships in piezoelectric and elastic layered systems should be examined. Recent studies have focused on the buckling, or loss of stability, of structures composed of piezoelectric materials [9-13].

The research initiated in paper [14] is furthered in paper [15], which investigates a PZT+Metal+PZT sandwich circular plate-disc with penny-shaped interface fractures exhibiting axisymmetric buckling delamination. As a result, the studies in papers [13,14] address the relevant 2D problems, while research on the three dimensional buckling delamination issues pertaining to elastic+piezoelectric layered systems remains entirely lacking. In view of the situation and the importance of investigating the relevant three dimensional problems, buckling delamination of a sandwich PZT+Metal+PZT plate with interface band cracks in [15], with interface edge cracks in [16], with two parallel interface-band cracks in [17] were investigated. In these three-dimensional analyses, a uniform uniaxial vertical force solely subjects the plate to compression from its two lateral surfaces.

Recent studies have also examined the post-buckling behavior of sandwich composite beams made of functionally graded material (FGM) faces and functionally graded porous (FGP) cores under high-temperature loads, providing insights into the thermal effects on stability [18]. Analyses on thermal vibration and stability of sandwich skew plates with functionally graded porous cores have further expanded the understanding of dynamic responses in such structures [19]. Additionally, the nonlinear transient response of sandwich beams with functionally graded porous cores under moving loads has been investigated, highlighting the importance of considering dynamic loading conditions [20]. Transient responses of sandwich plates with a functionally graded porous core have been studied using the Jacobi-Ritz method, offering alternative analytical approaches [21]. Dynamic analysis of functionally graded sandwich plates under multiple moving loads by the Ritz method with Gram-Schmidt polynomials has also been conducted, contributing to the development of more accurate predictive models [22].

In the current study, the three-dimensional buckling delamination mode of the embedded interface cracks of the thick piezoelectric sandwich plate under the effect of biaxial external pressure force in the direction of the cracks will be examined for various problem parameters.

2. Theory of the Problem

The exact field equations of Three-Dimensional Electro-Elasticity Theory and the piecewise homogeneous body model are used to create the mathematical model of the problem. Figure 1 illustrates the geometric configuration and loading conditions of the piezoelectric sandwich plate.

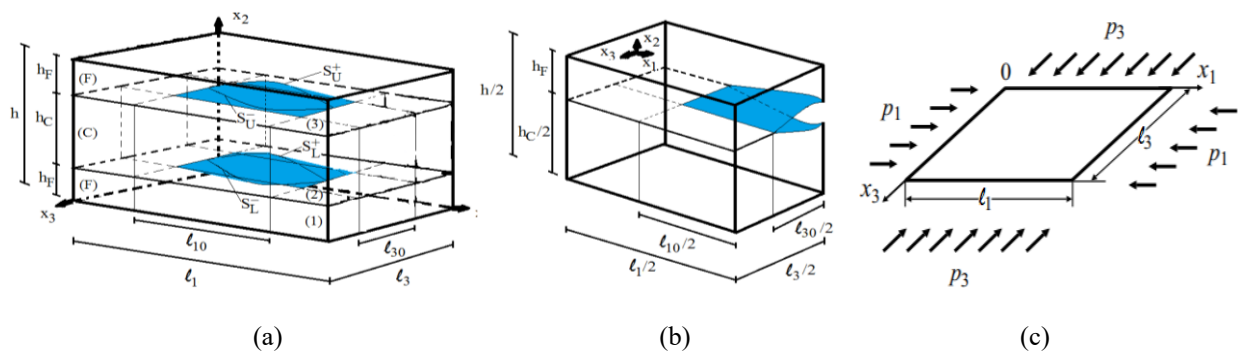

(a) (b) (c)

Fig. 1. The loading condition and the geometry of a rectangular thick plate with embedded cracks: (a) the entire solution domain, (b) one-eighth of the solution domain, (c) the loading statement.

The solution domain of the boundary value problem under consideration,

$$\Omega = \Omega_1 \cup \Omega_2 \cup \Omega_3 - S_L^{\mp} - S_U^{\mp} \tag{1}$$

where,

$$\begin{aligned} \Omega_1 &= \{0 \le x_1 \le \ell_1; 0 \le x_2 \le h_F; 0 \le x_3 \le \ell_3\}, \\ \Omega_2 &= \{0 \le x_1 \le \ell_1; h_F \le x_2 \le h_F + h_C; 0 \le x_3 \le \ell_3\}, \\ \Omega_3 &= \{0 \le x_1 \le \ell_1; h_F + h_C \le x_2 \le h; 0 \le x_3 \le \ell_3\}, \end{aligned} \tag{2}$$

$$\begin{aligned} S_L^{\mp} &= \{(\ell_1 - \ell_{10})/2 \le x_1 \le (\ell_1 + \ell_{10})/2; x_2 = h_F \mp 0; (\ell_3 - \ell_{30})/2 \le x_3 \le (\ell_3 + \ell_{30})/2\}, \\ S_U^{\mp} &= \{(\ell_1 - \ell_{10})/2 \le x_1 \le (\ell_1 + \ell_{10})/2; x_2 = h_F + h_C \mp 0; (\ell_3 - \ell_{30})/2 \le x_3 \le (\ell_3 + \ell_{30})/2\} \end{aligned} \tag{3}$$

In (1) Ω_1, Ω_2 and Ω_3 are the layers at the bottom, middle and top, respectively; $S_L^{\mp}(S_U^{\mp})$ are the lower (upper indices "-" i.e. $S_L^{-}(S_U^{-})$) and upper (upper indices "+" i.e. $S_L^{+}(S_U^{+})$) surfaces of the cracks located between lower and middle (middle and upper) layers (Fig. 1).

The 3D Electro-Elastic Plate Theory involves a set of field equations that couple both mechanical and electrical interactions in a material. This theory is commonly used to describe piezoelectric materials or electro-elastic systems where mechanical stress and deformation are influenced by electric fields and vice versa.

For the thick PZT rectangular sandwich plate with parallel identical rectangular between the layers of its face and core, the field equations applicable in the solution domain (1) can be articulated for each layer r_n $(n = 1,2,3)$ as follows.

$$\frac{\partial K_{ji}^{(r_n)}}{\partial x_j} = 0, \tag{4a}$$

$$\frac{\partial D_j^{(r_n)}}{\partial x_j} = 0, \tag{4b}$$

where,

$$K_{ji}^{(r_n)} = T_{jk}^{(r_n)}\left(\delta_i^k + \frac{\partial u_i^{(r_n)}}{\partial x_k}\right) + M_{ji}^{(r_n)}, D_i^{(r_n)} = e_{ikl}^{(r_n)} s_{kl}^{(r_n)} + \varepsilon_{ik}^{(r_n)} E_k^{(r_n)}$$

$$T_{ij}^{(r_n)} = c_{ijkl}^{(r_n)} s_{kl}^{(r_n)} - e_{kij}^{(r_n)} E_k^{(r_n)}, s_{kl}^{(r_n)} = \frac{1}{2}\left(\frac{\partial u_k^{(r_n)}}{\partial x_l} + \frac{\partial u_l^{(r_n)}}{\partial x_k} + \frac{\partial u_i^{(r_n)}}{\partial x_l}\frac{\partial u_i^{(r_n)}}{\partial x_k}\right)$$

$$M_{ji}^{(r_n)} = \varepsilon_0\left(E_i^{(r_n)} E_j^{(r_n)} - \frac{1}{2} E_k^{(r_n)} E_k^{(r_n)} \delta_i^j\right), E_k^{(r_n)} = -\frac{\partial \phi^{(r_n)}}{\partial x_k} \tag{4c}$$

(4a) and (4b) represents the mechanical equilibrium equations and electrical equilibrium equations respectively. In (4c), K_{ij} is the tangent stiffness matrix component; T_{jk} is stress tensor component; M_{ji} is Maxwell stress tensor component; u_i is mechanical displacement vector component; D_i is electrical displacement vector component; s_{kl} is Green strain tensor component; e_{ikl} is piezoelectrical constant; c_{ijkl} is elastic constant; ε_{ik} is dielectrical constant; E_k is electrical field component and ϕ is electrical potential. Also ε_0 denotes electrical permittivity, while δ_i^j represents Kronecker symbol.

It is presumed that the plate exhibits interface cracks, is simply supported along all lateral surfaces, and is exposed to static external pressure forces from $x_1 = 0; \ell_1$ and $x_3 = 0; \ell_3$ surfaces. Furthermore, it is presumed that no external force is exerted on the inferior and superior crack surfaces of the plate. Consequently, boundary conditions according to mechanical quantities are as given in Eq. (5).

$$\begin{aligned}
&u_2^{(r_n)}\big|_{x_1=0;\ell_1} = 0, u_2^{(r_n)}\big|_{x_3=0;\ell_3} = 0, K_{11}^{(r_n)}\big|_{x_1=0} = K_{11}^{(r_n)}\big|_{x_1=\ell_1} = p_1,\ K_{13}^{(r_n)}\big|_{x_1=0;\ell_1} = 0 \\
&K_{31}^{(r_n)}\big|_{x_3=0;\ell_3} = K_{33}^{(r_n)}\big|_{x_3=0;\ell_3} = p_3, K_{2i}^{(r_3)}\big|_{x_2=h} = K_{2i}^{(r_1)}\big|_{x_2=0} = 0, \\
&K_{ji}^{(r_3)}\big|_{S_U^+}\, n_{jU}^+ = K_{ji}^{(r_2)}\big|_{S_U^-}\, n_{jU}^- = 0, K_{ji}^{(r_2)}\big|_{S_L^+}\, n_{jL}^+ = K_{ji}^{(r_1)}\big|_{S_L^-}\, n_{jL}^- = 0
\end{aligned} \tag{5}$$

The electric potential is considered zero on all lateral surfaces of the PZT rectangular plate, indicating that these surfaces are insulating. The electrical displacement along the Ox_2 direction from the upper and lower surfaces of the PZT plates is presumed to be zero. Furthermore, it is acknowledged that the inside of the cracks are empty, constituting a vacuum. Boundary conditions based on the electrical quantities of these assumptions are given in Eq. (6).

$$\begin{aligned}
&\phi^{(r_n)}\big|_{x_1=0;\ell_1} = 0, \phi^{(r_n)}\big|_{x_3=0;\ell_3} = 0, D_2^{(r_1)}\big|_{x_2=0} = D_2^{(r_3)}\big|_{x_2=h} = 0, \\
&D_j^{(r_3)}\big|_{S_U^+}\, n_{jU}^+ = D_j^{(r_2)}\big|_{S_U^-}\, n_{jU}^- = 0, D_j^{(r_2)}\big|_{S_L^+}\, n_{jL}^+ = D_j^{(r_1)}\big|_{S_L^-}\, n_{jL}^- = 0
\end{aligned} \tag{6}$$

It is acknowledged that ideal contact conditions are attained between the layers of the sandwich thick plate in accordance with the mechanical and electrical quantities. Equation (7) specifies the contact conditions at the interface planes among the layers.

$$\begin{aligned}
&K_{2i}^{(r_1)}\big|_{x_2=h_F} = K_{2i}^{(r_2)}\big|_{x_2=h_F}, u_i^{(r_1)}\big|_{x_2=h_F} = u_i^{(r_2)}\big|_{x_2=h_F}, && \phi^{(r_1)}\big|_{x_2=h_F} = \phi^{(r_2)}\big|_{x_2=h_F}, D_2^{(r_1)}\big|_{x_2=h_F} = D_2^{(r_2)}\big|_{x_2=h_F}, \\
&K_{2i}^{(r_2)}\big|_{x_2=h_F+h_C} = K_{2i}^{(r_3)}\big|_{x_2=h_F+h_C}, u_i^{(r_2)}\big|_{x_2=h_F+h_C} = u_i^{(r_3)}\big|_{x_2=h_F+h_C}, && \phi^{(r_2)}\big|_{x_2=h_F+h_C} = \phi^{(r_3)}\big|_{x_2=h_F+h_C}, D_2^{(r_2)}\big|_{x_2=h_F+h_C} = D_2^{(r_3)}\big|_{x_2=h_F+h_C}
\end{aligned} \tag{7}$$

The boundary value problem addressed involves two embedded cracks given in Eqs. (1-7), which exemplify the buckling delamination problem arising around the cracks due to a uniformly distributed static external pressure force acting on all lateral edges of the piezoelectric sandwich rectangular thick plate. The problem addressed is nonlinear problem. The resolution of these nonlinear problems is simplified to the solution of linear series boundary value problems due to linearization methods [1]. According to the study referenced in [1], the desired magnitudes can be expressed in a serial form in relation to the dimensionless small parameter ε as follows:

$$\left\{\sigma_{ij}^{(r_n)}; \varepsilon_{ij}^{(r_n)}; u_i^{(r_n)}; D_i^{(r_n)}; E_i^{(r_n)}; \phi^{(r_n)}\right\} = \sum_{q=0}^{\infty} \varepsilon^q \left\{\sigma_{ij}^{(r_n),q}; \varepsilon_{ij}^{(r_n),q}; u_i^{(r_n),q}; D_i^{(r_n),q}; E_i^{(r_n),q}; \phi^{(r_n),q}\right\}, \varepsilon << 1. \tag{8}$$

For simplicity, each boundary value problem is designated based on the corresponding power of ε. For instance, they are referred to as zeroth, first, and so forth, boundary value problems or approximations. The resolution of the addressed buckling delamination issue is achieved using the superposition of the solutions derived from the series-boundary value issues utilizing (8).

To ascertain the critical external pressure force that causes delamination in the three-layered piezoelectric sandwich thick plate, it is enough to resolve solely the zeroth and first approaches from the series-boundary value issues derived using (8) [1]. Consequently, only the first two approximations from the series of boundary value problems derived using (8) will be addressed for this problem.

Each series boundary-value problem (approximation) derived from (8) encompasses the magnitudes of all prior approximations. Consequently, they cannot be resolved independently of one another. Approximations must be addressed sequentially, first with the zeroth approach. The zeroth approximation of the boundary value problem can be analytically resolved based on established mechanical and physical principles [1]. Consequently, the zeroth approximation is resolved analytically.

The solution for the first approximation of the boundary value problem is achieved numerically by three-dimensional finite element modeling. The solution domain is partitioned into finite elements shaped as rectangular prisms, with the electrical potential and displacements along the three axes treated as unknowns at the nodes.

$$\prod\left(u_1^{(r_n),1},u_2^{(r_n),1},u_3^{(r_n),1},\phi^{(r_n),1}\right)=\sum_{n=1}^{3}\iiint_{\Omega_n}\left[\frac{1}{2}G_{ijkl}^{(r_n),1}\frac{\partial u_i^{(r_n),1}}{\partial x_j}\frac{\partial u_k^{(r_n),1}}{\partial x_l}+R_{ijk}^{(r_n)}\frac{\partial \phi^{(r_n),1}}{\partial x_i}\frac{\partial u_j^{(r_n),1}}{\partial x_k}-\right.$$

$$\left.\frac{1}{2}\varepsilon_{ij}^{(r_n)}\frac{\partial \phi^{(r_n),1}}{\partial x_k}\frac{\partial \phi^{(r_n),1}}{\partial x_l}\right]d\Omega_n-\iint_{S_L^-}T_{11}^{(1),0}\frac{\partial f^-(x_1)}{\partial x_1}u_1^{(1),1}\Big|_{x_2=h_F-0}dx_1dx_3-\iint_{S_L^-}T_{33}^{(1),0}\frac{\partial f^-(x_1)}{\partial x_3}u_3^{(1),1}\Big|_{x_2=h_F-0}dx_1dx_3$$

$$\iint_{S_L^+}T_{11}^{(2),0}\frac{\partial f^-(x_1)}{\partial x_1}u_1^{(2),1}\Big|_{x_2=h_F+0}dx_1dx_3-\iint_{S_L^+}T_{33}^{(2),0}\frac{\partial f^-(x_1)}{\partial x_3}u_3^{(2),1}\Big|_{x_2=h_F+0}dx_1dx_3-$$

$$\iint_{S_U^-}T_{11}^{(2),0}\frac{\partial f^-(x_1)}{\partial x_1}u_1^{(2),1}\Big|_{x_2=h_F+h_C-0}dx_1dx_3-\iint_{S_U^-}T_{33}^{(2),0}\frac{\partial f^-(x_1)}{\partial x_3}u_3^{(2),1}\Big|_{x_2=h_F+h_C-0}dx_1dx_3-$$

$$\iint_{S_U^+}T_{11}^{(3),0}\frac{\partial f^-(x_1)}{\partial x_1}u_1^{(3),1}\Big|_{x_2=h_F+h_C+0}dx_1dx_3-\iint_{S_U^+}T_{33}^{(3),0}\frac{\partial f^-(x_1)}{\partial x_3}u_3^{(3),1}\Big|_{x_2=h_F+h_C+0}dx_1dx_3-$$

$$-\iint_{S_L^-}D_1^{(1),0}\frac{\partial f^-(x_1)}{\partial x_1}\phi^{(1),1}\Big|_{x_2=h_F-0}dx_1dx_3-\iint_{S_L^+}D_1^{(2),0}\frac{\partial f^-(x_1)}{\partial x_1}\phi^{(2),1}\Big|_{x_2=h_F+0}dx_1dx_3-$$

$$\iint_{S_U^-}D_1^{(2),0}\frac{\partial f^-(x_1)}{\partial x_1}\phi^{(2),1}\Big|_{x_2=h_F+h_C-0}dx_1dx_3-\iint_{S_U^+}D_1^{(3),0}\frac{\partial f^-(x_1)}{\partial x_1}\phi^{(3),1}\Big|_{x_2=h_F+h_C+0}dx_1dx_3 \tag{9}$$

The functional representing the total electro-mechanical energy accumulated in the item is utilized for finite element modeling [23, 24]. Utilizing the established Ritz technique outlined in (9), the solution of the problem is simplified to solving an algebraic equations system. Our objective is to identify the delamination buckling modes that arise around cracks; however, it is essential first to ascertain the crucial delamination force that induces delamination buckling in the plate.

$$\left|u_2^{(3),1}\Big|_{\substack{x_2=h_F+h_C+0\\x_1=\ell_1/2}}\right|\to+\infty\ \text{ as }\ p_1\to p_{cr} \tag{10}$$

The critical external pressure force values that induce delamination buckling around the cracks in the analyzed piezoelectric rectangular thick plate are identified by iterative methods as outlined in Eq. (10). Subsequently, the graphs for the crack surface buckling mode are established for the specified external force ($p < p_{cr}$).

$$f(x_1,x_3)=A\ell_{10}\sin^2\left(\frac{\pi}{\ell_{10}}\left(x_1-\frac{\ell_1-\ell_{10}}{2}\right)\right)\sin^2\left(\frac{\pi}{\ell_{30}}\left(x_3-\frac{\ell_3-\ell_{30}}{2}\right)\right) \tag{11}$$

Eq. (11) provides the analytical formula for the function indicating the pre-slope configuration allocated to the crack surfaces before actual loading, based on the small initial imperfection criterion. A is a constant in this case.

Before proceeding to numerical results, the following flowchart has been followed for solving the problem:

Step 1: Define Geometry and Material Properties - Plate thickness, dimensions, material properties (elastic constants, piezoelectric constants, dielectric constants) - Boundary conditions - Meshing the domain (discretization into finite elements)

Step 2: Set Up Governing Equations - Mechanical equations: stress-strain relations - Electrical equations: Maxwell equations, piezoelectric relations

Step 3: Define the analytical solution of the zeroth approximation. - Discretize the equations (Finite Element Analysis) for the first approximation. Generate a stiffness matrix for mechanical and electrical components. - Discretize the domain into small elements (using the finite element method, FEM). - Apply piezoelectric coupling terms in the FEM formulation.

Step 4: Apply Boundary and Initial Conditions - Apply mechanical boundary conditions (displacements, forces). - Apply electrical boundary conditions (electric potential, electric field).

Step 5: Solve the System of Equations - Assemble a global stiffness matrix for mechanical and electrical systems. - Solve the system of equations for the critical value of p caused by buckling delamination using MATLAB.

Step 6: Extract and plot results: displacement field and piezoelectric coupling effects—Visualize results using MATLAB plotting tools.

Step 7: Analyze and Interpret Results

3. Discussion of The Numerical Results

Numerical analyses are conducted for the case in which the face layers consist of piezoelectric materials, whereas the core layer is composed of elastic material (metal). The open-circuit condition is fulfilled at the surface planes of the piezoelectric layers in contact with the core layer. Numerical analyses reveal that PZT-5H is employed for the face layers, whereas steel (St) and aluminum (Al) serve as the core layer elements. The electro-mechanical material constants of PZT-5H utilized in the numerical computations are presented in Table 1.

Table 1: Electro-mechanical properties of PZT-5H material [23]

$c_{11}^{(r_1)}$	$c_{12}^{(r_1)}$	$c_{13}^{(r_1)}$	$c_{33}^{(r_1)}$	$c_{44}^{(r_1)}$	$c_{66}^{(r_1)}$	$e_{31}^{(r_1)}$	$e_{33}^{(r_1)}$	$e_{15}^{(r_1)}$	$\varepsilon_{11}^{(r_1)}$	$\varepsilon_{33}^{(r_1)}$
12.6	7.91	8.39	11.7	2.30	2.35	-6.5	23.3	17.0	1.505	1.302
		$\times 10^{10}$ N/m^2					C/m^2		$\times 10^{-8}$ C/Vm	

The mechanical properties of the metallic materials are presented as follows: λ_{Al}=48.1 GPa, μ_{Al}=27.1 GPa and λ_{St}=92.6 GPa, μ_{St}=77.5 GPa, where λ and μ represent the Lame constants of the materials. The material constants for the middle layer as follows:

$$c_{11} = \lambda + 2\mu,\ c_{22} = c_{33} = c_{11},\ \ c_{12} = c_{21} = \lambda,\ \ c_{13} = c_{31} = \lambda,\ c_{23} = c_{32} = \lambda,\ c_{66} = \mu,\ \ c_{44} = c_{55} = c_{66} \tag{12}$$

All investigations conducted in this study assume that the polarization direction of the piezoelectric material aligns with the Ox_2 axis. Prior to analyzing the numerical results derived from the topic at hand, the precision of the methods and programs utilized in our numerical investigations is verified using test problems. The relevant critical force values for the isotropic rectangular thick plate, as shown in [2], are detailed in Table 2 for the parameters $(h/\ell_1 = 0.15, \ell_{10}/\ell_1 = 0.5, \ell_{30}/\ell_1 = 0.5)$.

Along the Ox_1, Ox_2 and Ox_3 axes, the solution domain is partitioned into 100, 24 and 100 finite elements, respectively. In order to build the finite element mesh, the convergence criterion regarding the critical force is employed, whereby the effect of any additional increase in the finite element count does not exceed 10^{-5}. All algorithms and programs utilized to derive the results presented in Table 2, as well as the subsequent results to be addressed, are developed by the authors of this research and implemented in MATLAB.

The results indicate that the critical delamination buckling force values diminished as the ratio of the coaxial compressive force values, i.e., (p_3/p_1) increases. The critical delamination buckling force values diminish as the parameter h_F/ℓ_1 decreases. The results for each parameter value, as illustrated in Table 2, align with the established results in the literature. This provides confidence in the algorithms and programs created by us.

Table 2: $p_{cr} / \mu\left(\frac{E}{2(1+\nu)}\right)$ critical buckling delamination forces for the isotropic rectangular thick plate.

p_3 / p_1	h_F / ℓ_1							
	This study				[2]			
	0.05	0.0375	0.025	0.0125	0.05	0.0375	0.025	0.0125
0	0.0684	0.0451	0.0251	0.0112	0.0684	0.0451	0.0251	0.0111
0.5	0.0488	0.0319	0.0176	0.0078	0.0488	0.0319	0.0176	0.0077
1	0.0369	0.0241	0.0133	0.0058	0.0369	0.0241	0.0133	0.0058

To ascertain the influence of electro-mechanical connection on the critical delamination buckling force values, Numerical results are acquired for two separate cases.

Case1: The piezoelectric coefficients of the materials are established as zero, i.e., $(e_{ij} = \varepsilon_{ij} = 0)$

Case2: The piezoelectric coefficients of the materials are established as non-zero, i.e., $(e_{ij} \neq 0, \varepsilon_{ij} \neq 0)$.

Tables 3 to 6 present the critical delamination buckling force values derived from the solution of the problem, considering various material combinations, crack lengths, and compressive force ratios. The tables present the acquired material pairs of PZT-5H/St/PZT-5H (Tables 3 and 4) and PZT-5H/Al/PZT-5H (Tables 5 and 6), includingvarying crack lengths and pressure force ratios. Numerical results are provided for the parameters $h / \ell_1 = 0.2$, $h_F / \ell_1 = 0.05$, $\ell_{30} / \ell_1 = 0.5$. The numerical results of ignoring the piezoelectric and dielectric effects i.e., for Case 1, as shown in Tables 4 and 6, and including them i.e., for Case 2, as indicated in Tables 3 and 5, are also provided.

The results indicate that the critical delamination buckling force values diminish as the ratio of the coaxial compressive force, i.e., (p_3 / p_1), and also as the internal crack length, i.e., (ℓ_{10} / ℓ_1). The critical delamination buckling values for Case 1 are inferior to those for Case 2. A contrast of the results for plates with core layers composed of aluminum and steel indicates that the critical delamination buckling values for plates with the steel core layer surpass those of the aluminum core layer.

Table 3: Critical pressure force values inducing delamination buckling in a PZT-5H/St/PZT-5H sandwich plate for Case 1.

p_3 / p_1	ℓ_{10} / ℓ_1								
	0.3	0.35	0.4	0.45	0.5	0.55	0.6	0.65	0.7
0	0.3160	0.2901	0.2750	0.2695	0.2667	0.2606	0.2571	0.2433	0.2378
0.3	0.2235	0.2004	0.1813	0.1757	0.1705	0.1650	0.1618	0.1547	0.1503
0.5	0.1986	0.1822	0.1602	0.1521	0.1490	0.1423	0.1379	0.1319	0.1251
0.7	0.1735	0.1632	0.1471	0.1363	0.1319	0.1247	0.1197	0.1127	0.1093
1	0.1509	0.1359	0.1243	0.1173	0.1120	0.1048	0.0996	0.0912	0.0885

Table 4: Critical pressure force values inducing delamination buckling in a PZT-5H/St/PZT-5H sandwich plate for Case 2.

p_3 / p_1	ℓ_{10} / ℓ_1								
	0.3	0.35	0.4	0.45	0.5	0.55	0.6	0.65	0.7
0	0.6285	0.5897	0.5581	0.5512	0.5434	0.5221	0.5084	0.4772	0.4635
0.3	0.4862	0.4428	0.4222	0.4102	0.3877	0.3663	0.3491	0.3387	0.3253
0.5	0.4572	0.4203	0.4113	0.3957	0.3667	0.3453	0.3213	0.3072	0.2957
0.7	0.4332	0.4059	0.3952	0.3702	0.3475	0.3221	0.2902	0.2796	0.2662
1	0.4031	0.3883	0.3755	0.3477	0.3202	0.2955	0.2673	0.2503	0.2352

Table 5: Critical pressure force values inducing delamination buckling in a PZT-5H/Al/PZT-5H sandwich plate for Case 1.

p_3 / p_1	ℓ_{10} / ℓ_1								
	0.3	0.35	0.4	0.45	0.5	0.55	0.6	0.65	0.7
0	0.2557	0.2372	0.2115	0.2087	0.2003	0.1993	0.1972	0.1902	0.1887
0.3	0.2076	0.1915	0.1702	0.1633	0.1579	0.1462	0.1286	0.1199	0.1162
0.5	0.1897	0.1763	0.1575	0.1487	0.1402	0.1257	0.1175	0.1003	0.0992
0.7	0.1677	0.1573	0.1422	0.1353	0.1322	0.1113	0.1012	0.0871	0.0752
1	0.1396	0.1287	0.1198	0.1122	0.1076	0.0973	0.0897	0.0697	0.0563

Table 6: Critical pressure force values inducing delamination buckling in a PZT-5H/Al/PZT-5H sandwich plate for Case 2.

p_3 / p_1	ℓ_{10} / ℓ_1								
	0.3	0.35	0.4	0.45	0.5	0.55	0.6	0.65	0.7
0	0.5297	0.4802	0.4385	0.4275	0.4122	0.4082	0.4053	0.3973	0.3869
0.3	0.4113	0.3898	0.3673	0.3415	0.3159	0.2913	0.2798	0.2665	0.2467
0.5	0.3873	0.3565	0.3229	0.3097	0.2812	0.2657	0.2433	0.2302	0.2112
0.7	0.3621	0.3340	0.3013	0.2850	0.2410	0.2217	0.2063	0.1987	0.1895
1	0.3310	0.2976	0.2765	0.2462	0.2169	0.2058	0.1942	0.1812	0.1603

In [11], the buckling delamination problem of a piezoelectric sandwich strip plate (PZT/Al/PZT) was experimentally studied by Giannopoulos and others. In this article, the critical force values obtained for the open circuit (here, Case 2) are greater than those for the closed circuit (here, Case 1). This is consistent with the numerical results obtained here (Table 3-Table 4 and Table 5-Table 6).

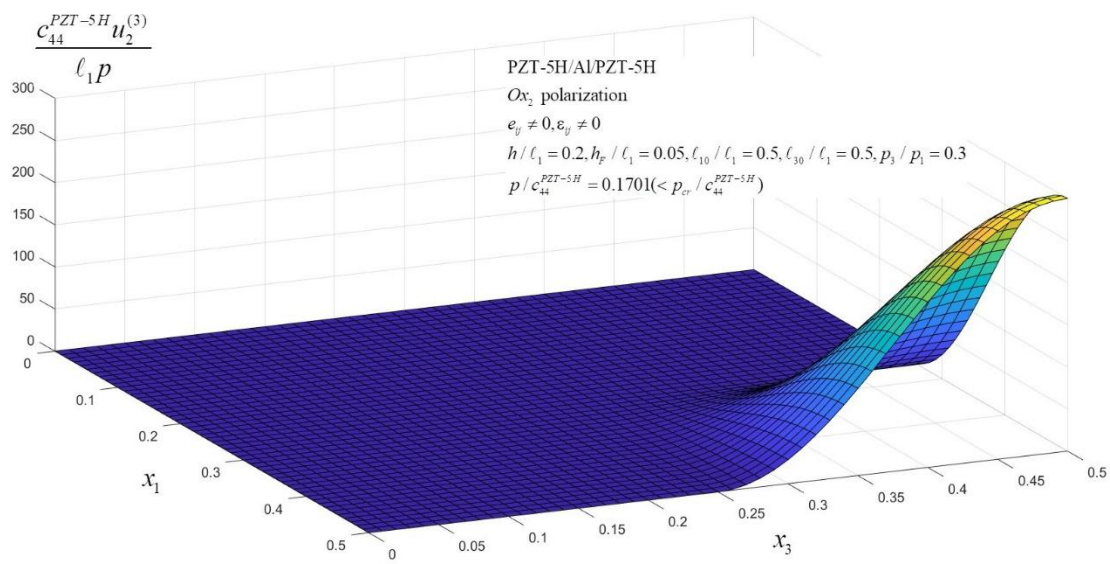

Fig. 2. The buckling mode of the PZT-5H/Al/PZT-5H plate with an embedded crack under the influence of the biaxial external pressure forces for $p = 0.1701 (< p_{cr} / c_{44}^{PZT-5H})$

Ultimately, we examine the illustrations presented in Fig. 2 and 3, which exemplify the buckling delamination mode, i.e., $u_2^{(3)} c_{44}^{PZT-5H} / \ell_1 p$. This mode is designed for the PZT-5H/Al/PZT-5H plate under $h/\ell_1 = 0.2$, $h_F/\ell_1 = 0.05$, $\ell_{10}/\ell_1 = 0.5$ and $\ell_{30}/\ell_1 = 0.5$, in the case where $p = 0.1701 (< p_{cr} / c_{44}^{PZT-5H})$ for Figure 2 and

$p = 0.1706(> p_{cr} / c_{44}^{PZT-5H})$ for Fig. 3. As the external compressive force approaches its critical limits, the surface displacement values significantly increase. The data demonstrate that the buckling delamination mode of the face planes corresponds with existing mechanical principles, the initial imperfections of the cracks' edge surfaces, and the boundary conditions defined on the lateral edge planes of the plates. It has been determined that the form of the initial imperfection given by (11) to the crack surfaces before the external force acts on the plate under consideration is similar to the crack surface form obtained in Figure 2 and in Figure 3. It is noted that under the effect of external pressure, the cracks opened in accordance with the infinitesimal initial imperfection criterion present on the crack surfaces.

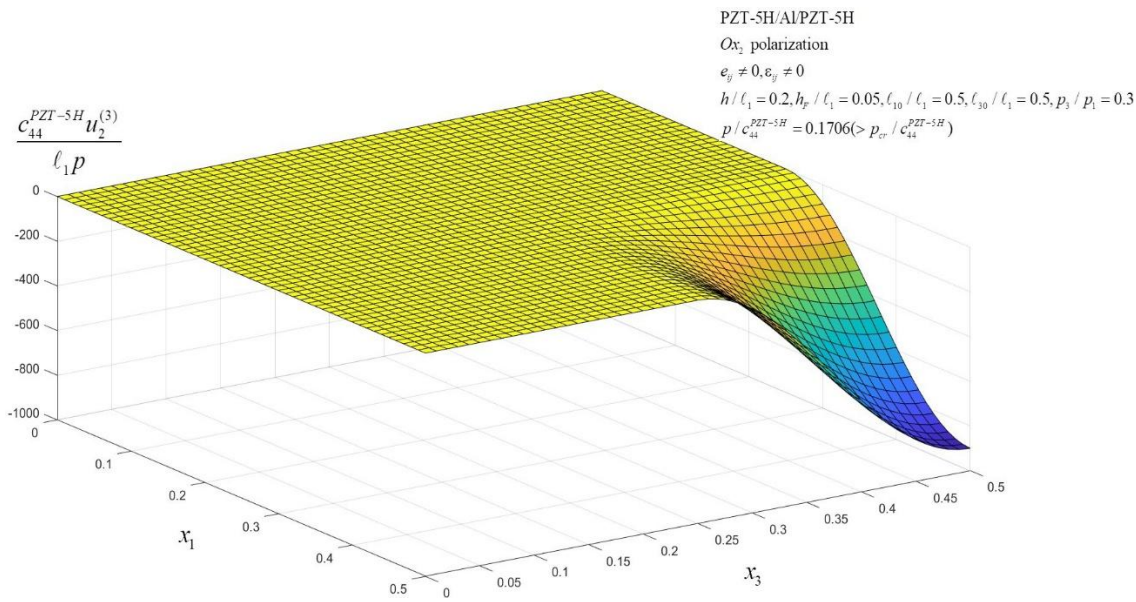

Fig. 3. The buckling mode of the PZT-5H/Al/PZT-5H plate with an embedded crack under the influence of the biaxial external pressure forces for $p = 0.1706(> p_{cr} / c_{44}^{PZT-5H})$

4. Conclusion

This study examines the buckling delamination problems that arise around cracks under uniformly distributed static external biaxial pressure applied from opposite edges of the plate, with piezoelectric face layers and a metallic core layer containing rectangular embedded cracks between the layers. The edges of embedded cracks are presumed to possess infinitesimal initial imperfections. The progression of this imperfection is analyzed when the absolute values of these forces increase, employing the criterion of critical compressive force in an incident where the displacement of the crack edges becomes infinite. The novel scientific conclusions derived from this research can be encapsulated as follows:

- The piezoelectric characteristics of the materials in the face layers lead to increased critical force values,
- The critical delamination buckling forces decrease with increasing coaxial compressive force ratio and internal crack length,
- Case 2's critical delamination buckling forces, factoring in piezoelectric and dielectric constants, exceed those of Case 1, which ignores them,
- The contrast of plates with aluminum and steel core layers indicates that steel core plates have greater critical delamination buckling values.

References

[1] Akbarov SD. Stability loss and buckling delamination: Three-dimensional linearized approach for elastic and viscoelastic composites. Heidelberg, New York: Springer; 2013.

[2] Akbarov SD, Yahnioglu N, Tekin A. Buckling delamination of a rectangular sandwich plate containing inner cracks under biaxial loading. Mechanics of Composite Materials. 2013;49(5):537–550.

[3] Akbarov SD, Yahnioglu N, Tekin A. Buckling delamination of a rectangular viscoelastic sandwich plate containing interface inner cracks. Journal of Engineering Mechanics. 2014;140(1):134–148.
[4] Szekrényes A. Analytical solution of some delamination scenarios in thick structural sandwich plates. Journal of Sandwich Structures and Materials. 2019;21(4):1271–1315.
[5] Shishesaz M, Mahsa K, Hosseini P, Hosseini M. Buckling behavior of composite plates with a pre-central circular delamination defect under in-plane uniaxial compression. Journal of Computational and Applied Mechanics. 2017;48:111–122.
[6] Frostig Y, Sokolinsky V. Higher-order buckling of debonded (delaminated) sandwich panels with soft core. AIAA Journal. 2000;38:2147–2159.
[7] Rao SS, Sunar M. Piezoelectricity and its use in disturbance sensing and control of flexible structures: A survey. Applied Mechanics Reviews. 1994;47:113–123.
[8] Li YL, Fu YM, Dai HL. Postbuckling and delamination growth for delaminated piezoelectric elastoplastic laminated beams under hygrothermal conditions. Journal of Mechanics of Materials and Structures. 2012;7(1):85–102.
[9] Yang JS. Buckling of a piezoelectric plate. International Journal of Solids and Structures. 1998;44:399–408.
[10] Hu YT, Yang JS, Jiang Q. A model for electroelastic plates under biasing fields with applications in buckling analysis. International Journal of Solids and Structures. 2002;39:2629–2642.
[11] Giannopoulos G, Santafe F, Vantomme J. Thermal, electrical, and mechanical coupled mechanics for initial buckling analysis of smart plates and beams using discrete layer kinematics. International Journal of Solids and Structures. 2007;44:4707–4722.
[12] Jerome R, Ganesan N. New generalized plane strain finite element formulation for the buckling analysis of piezocomposite beam. Finite Elements in Analysis and Design. 2010;46:896–904.
[13] Akbarov SD, Yahnioglu N. Buckling delamination of a sandwich plate-strip with piezoelectric face and elastic core layers. Applied Mathematical Modelling. 2013;37(16–17):8029–8038.
[14] Cafarova FI, Akbarov SD, Yahnioglu N. Buckling delamination of the PZT/Metal/PZT sandwich circular plate-disc with penny-shaped interface cracks. Smart Structures and Systems. 2017;19(2):163–179.
[15] Aylikci F, Akbarov SD, Yahnioglu N. Buckling delamination of a PZT/Metal/PZT sandwich rectangular thick plate containing interface inner band cracks. Composite Structures. 2018;202:9–16.
[16] Aylikci F, Yahnioglu N. The effect of crack size on the buckling delamination mode (surface wrinkles) of a piezoelectric sandwich rectangular thick plate with interface edge cracks. AIP Conference Proceedings. 2018;2042:020048.
[17] Aylikci F, Yahnioglu N, Elibol A. Finite element method analysis of the influence of the plate geometry on the buckling delamination of a piezoelectric sandwich rectangular thick plate. Sigma Journal of Engineering and Natural Sciences. 2018;9(2):193–202.
[18] Vessakosol P, Eiadtrong S, Thai S, Wattanasakulpong N. Post-buckling behavior of sandwich composite beams made of functionally graded material faces and functionally graded porous core under high-temperature loads. International Journal of Structural Stability and Dynamics. 2025;25:2550193.
[19] Wattanasakulpong N, Thai S, Eiadtrong S. Analyses on thermal vibration and stability of sandwich skew plates with functionally graded porous core. Thin-Walled Structures. 2023;58:105536.
[20] Songsuwan W, Wattanasakulpong N, Kumar S. Nonlinear transient response of sandwich beams with functionally graded porous core under moving load. Engineering Analysis with Boundary Elements. 2023;155:11–24.
[21] Wattanasakulpong N, Eiadtrong S. Transient responses of sandwich plates with a functionally graded porous core using Jacobi–Ritz method. International Journal of Structural Stability and Dynamics. 2023;23(4):2350039.
[22] Songsuwan W, Wattanasakulpong N, Pimsarn M. Dynamic analysis of functionally graded sandwich plates under multiple moving loads by Ritz method with Gram–Schmidt polynomials. International Journal of Structural Stability and Dynamics. 2021;21(10):2150138.
[23] Yang J. An introduction to the theory of piezoelectricity. Springer; 2005.
[24] Tiersten HF. Linear piezoelectric plate vibrations. New York, NY: Plenum; 1969.

Appendix

$$K_{ij}^{(e)}(1,1)=\int_{-1}^{1}\int_{-1}^{1}\int_{-1}^{1}\left(\left(c_{11}^{(r_n)}+T_{11}^{(r_n),0}\right)\frac{\partial N_i}{\partial\xi}\frac{\partial N_j}{\partial\eta}+c_{55}^{(r_n)}\frac{\partial N_i}{\partial\zeta}\frac{\partial N_j}{\partial\zeta}+c_{66}^{(r_n)}\frac{\partial N_i}{\partial\eta}\frac{\partial N_j}{\partial\eta}\right)Jd\xi d\eta d\zeta,$$

$$K_{ij}^{(e)}(1,2)=\int_{-1}^{1}\int_{-1}^{1}\int_{-1}^{1}\left(\left(c_{66}^{(r_n)}+T_{22}^{(r_n),0}\right)\frac{\partial N_i}{\partial\eta}\frac{\partial N_j}{\partial\xi}+c_{12}^{(r_n)}\frac{\partial N_i}{\partial\xi}\frac{\partial N_j}{\partial\eta}\right)Jd\xi d\eta d\zeta,$$

$$K_{ij}^{(e)}(1,3)=\int_{-1}^{1}\int_{-1}^{1}\int_{-1}^{1}\left(\left(c_{55}^{(r_n)}+T_{33}^{(r_n),0}\right)\frac{\partial N_i}{\partial\zeta}\frac{\partial N_j}{\partial\xi}+c_{13}^{(r_n)}\frac{\partial N_i}{\partial\xi}\frac{\partial N_j}{\partial\zeta}\right)Jd\xi d\eta d\zeta,$$

$$\begin{aligned}K_{ij}^{(e)}(1,4)=\int_{-1}^{1}\int_{-1}^{1}\int_{-1}^{1}\Bigg(&e_{11}^{(r_n)}\frac{\partial N_i}{\partial\xi}\frac{\partial N_j}{\partial\xi}+e_{16}^{(r_n)}\frac{\partial N_i}{\partial\eta}\frac{\partial N_j}{\partial\xi}+e_{15}^{(r_n)}\frac{\partial N_i}{\partial\zeta}\frac{\partial N_j}{\partial\xi}\\&+e_{21}^{(r_n)}\frac{\partial N_i}{\partial\xi}\frac{\partial N_j}{\partial\eta}+e_{26}^{(r_n)}\frac{\partial N_i}{\partial\eta}\frac{\partial N_j}{\partial\eta}+e_{25}^{(r_n)}\frac{\partial N_i}{\partial\zeta}\frac{\partial N_j}{\partial\eta}\\&+e_{31}^{(r_n)}\frac{\partial N_i}{\partial\xi}\frac{\partial N_j}{\partial\zeta}+e_{36}^{(r_n)}\frac{\partial N_i}{\partial\eta}\frac{\partial N_j}{\partial\zeta}+e_{35}^{(r_n)}\frac{\partial N_i}{\partial\zeta}\frac{\partial N_j}{\partial\zeta}\Bigg)Jd\xi d\eta d\zeta,\end{aligned}$$

$$K_{ij}^{(e)}(2,1)=\int_{-1}^{1}\int_{-1}^{1}\int_{-1}^{1}\left(\left(c_{66}^{(r_n)}+T_{22}^{(r_n),0}\right)\frac{\partial N_i}{\partial\xi}\frac{\partial N_j}{\partial\eta}+c_{12}^{(r_n)}\frac{\partial N_i}{\partial\eta}\frac{\partial N_j}{\partial\xi}\right)Jd\xi d\eta d\zeta,$$

$$K_{ij}^{(e)}(2,2)=\int_{-1}^{1}\int_{-1}^{1}\int_{-1}^{1}\left(\left(c_{22}^{(r_n)}+T_{22}^{(r_n),0}\right)\frac{\partial N_i}{\partial\eta}\frac{\partial N_j}{\partial\eta}+c_{44}^{(r_n)}\frac{\partial N_i}{\partial\zeta}\frac{\partial N_j}{\partial\zeta}+\left(c_{66}^{(r_n)}+T_{11}^{(r_n),0}\right)\frac{\partial N_i}{\partial\xi}\frac{\partial N_j}{\partial\xi}\right)Jd\xi d\eta d\zeta,$$

$$K_{ij}^{(e)}(2,3)=\int_{-1}^{1}\int_{-1}^{1}\int_{-1}^{1}\left(\left(c_{44}^{(r_n)}+T_{33}^{(r_n),0}\right)\frac{\partial N_i}{\partial\zeta}\frac{\partial N_j}{\partial\eta}+c_{23}^{(r_n)}\frac{\partial N_i}{\partial\eta}\frac{\partial N_j}{\partial\zeta}\right)Jd\xi d\eta d\zeta,$$

$$\begin{aligned}K_{ij}^{(e)}(2,4)=\int_{-1}^{1}\int_{-1}^{1}\int_{-1}^{1}\Bigg(&e_{16}^{(r_n)}\frac{\partial N_i}{\partial\xi}\frac{\partial N_j}{\partial\xi}+e_{12}^{(r_n)}\frac{\partial N_i}{\partial\eta}\frac{\partial N_j}{\partial\xi}+e_{14}^{(r_n)}\frac{\partial N_i}{\partial\zeta}\frac{\partial N_j}{\partial\xi}\\&+e_{26}^{(r_n)}\frac{\partial N_i}{\partial\xi}\frac{\partial N_j}{\partial\eta}+e_{22}^{(r_n)}\frac{\partial N_i}{\partial\eta}\frac{\partial N_j}{\partial\eta}+e_{24}^{(r_n)}\frac{\partial N_i}{\partial\zeta}\frac{\partial N_j}{\partial\eta}\\&+e_{36}^{(r_n)}\frac{\partial N_i}{\partial\xi}\frac{\partial N_j}{\partial\zeta}+e_{32}^{(r_n)}\frac{\partial N_i}{\partial\eta}\frac{\partial N_j}{\partial\zeta}+e_{34}^{(r_n)}\frac{\partial N_i}{\partial\zeta}\frac{\partial N_j}{\partial\zeta}\Bigg)Jd\xi d\eta d\zeta,\end{aligned}$$

$$K_{ij}^{(e)}(3,1)=\int_{-1}^{1}\int_{-1}^{1}\int_{-1}^{1}\left(\left(c_{55}^{(r_n)}+T_{33}^{(r_n),0}\right)\frac{\partial N_i}{\partial\xi}\frac{\partial N_j}{\partial\zeta}+c_{13}^{(r_n)}\frac{\partial N_i}{\partial\zeta}\frac{\partial N_j}{\partial\xi}\right)Jd\xi d\eta d\zeta,$$

$$K_{ij}^{(e)}(3,2)=\int_{-1}^{1}\int_{-1}^{1}\int_{-1}^{1}\left(\left(c_{44}^{(r_n)}+T_{33}^{(r_n),0}\right)\frac{\partial N_i}{\partial\eta}\frac{\partial N_j}{\partial\zeta}+c_{23}^{(r_n)}\frac{\partial N_i}{\partial\zeta}\frac{\partial N_j}{\partial\eta}\right)Jd\xi d\eta d\zeta,$$

$$K_{ij}^{(e)}(3,3)=\int_{-1}^{1}\int_{-1}^{1}\int_{-1}^{1}\left(c_{33}^{(r_n)}\frac{\partial N_i}{\partial\zeta}\frac{\partial N_j}{\partial\zeta}+\left(c_{55}^{(r_n)}+T_{11}^{(r_n),0}\right)\frac{\partial N_i}{\partial\xi}\frac{\partial N_j}{\partial\xi}+c_{44}^{(r_n)}\frac{\partial N_i}{\partial\eta}\frac{\partial N_j}{\partial\eta}\right)Jd\xi d\eta d\zeta,$$

$$\begin{aligned}K_{ij}^{(e)}(3,4)=\int_{-1}^{1}\int_{-1}^{1}\int_{-1}^{1}\Bigg(&e_{15}^{(r_n)}\frac{\partial N_i}{\partial\xi}\frac{\partial N_j}{\partial\xi}+e_{14}^{(r_n)}\frac{\partial N_i}{\partial\eta}\frac{\partial N_j}{\partial\xi}+e_{13}^{(r_n)}\frac{\partial N_i}{\partial\zeta}\frac{\partial N_j}{\partial\xi}\\&+e_{25}^{(r_n)}\frac{\partial N_i}{\partial\xi}\frac{\partial N_j}{\partial\eta}+e_{24}^{(r_n)}\frac{\partial N_i}{\partial\eta}\frac{\partial N_j}{\partial\eta}+e_{23}^{(r_n)}\frac{\partial N_i}{\partial\zeta}\frac{\partial N_j}{\partial\eta}\\&+e_{35}^{(r_n)}\frac{\partial N_i}{\partial\xi}\frac{\partial N_j}{\partial\zeta}+e_{34}^{(r_n)}\frac{\partial N_i}{\partial\eta}\frac{\partial N_j}{\partial\zeta}+e_{33}^{(r_n)}\frac{\partial N_i}{\partial\zeta}\frac{\partial N_j}{\partial\zeta}\Bigg)Jd\xi d\eta d\zeta,\end{aligned}$$

$$\begin{aligned}K_{ij}^{(e)}(4,1)=\int_{-1}^{1}\int_{-1}^{1}\int_{-1}^{1}\Bigg(&e_{11}^{(r_n)}\frac{\partial N_i}{\partial\xi}\frac{\partial N_j}{\partial\xi}+e_{16}^{(r_n)}\frac{\partial N_i}{\partial\eta}\frac{\partial N_j}{\partial\xi}+e_{15}^{(r_n)}\frac{\partial N_i}{\partial\zeta}\frac{\partial N_j}{\partial\xi}\\&+e_{21}^{(r_n)}\frac{\partial N_i}{\partial\xi}\frac{\partial N_j}{\partial\eta}+e_{26}^{(r_n)}\frac{\partial N_i}{\partial\eta}\frac{\partial N_j}{\partial\eta}+e_{25}^{(r_n)}\frac{\partial N_i}{\partial\zeta}\frac{\partial N_j}{\partial\eta}\\&+e_{31}^{(r_n)}\frac{\partial N_i}{\partial\xi}\frac{\partial N_j}{\partial\zeta}+e_{36}^{(r_n)}\frac{\partial N_i}{\partial\eta}\frac{\partial N_j}{\partial\zeta}+e_{35}^{(r_n)}\frac{\partial N_i}{\partial\zeta}\frac{\partial N_j}{\partial\zeta}\Bigg)Jd\xi d\eta d\zeta,\end{aligned}$$

$$K_{ij}^{(e)}(4,2)=\int_{-1}^{1}\int_{-1}^{1}\int_{-1}^{1}\Bigg(e_{16}^{(r_n)}\frac{\partial N_i}{\partial\xi}\frac{\partial N_j}{\partial\xi}+e_{12}^{(r_n)}\frac{\partial N_i}{\partial\eta}\frac{\partial N_j}{\partial\xi}+e_{14}^{(r_n)}\frac{\partial N_i}{\partial\zeta}\frac{\partial N_j}{\partial\xi}$$
$$+e_{26}^{(r_n)}\frac{\partial N_i}{\partial\xi}\frac{\partial N_j}{\partial\eta}+e_{22}^{(r_n)}\frac{\partial N_i}{\partial\eta}\frac{\partial N_j}{\partial\eta}+e_{24}^{(r_n)}\frac{\partial N_i}{\partial\zeta}\frac{\partial N_j}{\partial\eta}$$
$$+e_{36}^{(r_n)}\frac{\partial N_i}{\partial\xi}\frac{\partial N_j}{\partial\zeta}+e_{32}^{(r_n)}\frac{\partial N_i}{\partial\eta}\frac{\partial N_j}{\partial\zeta}+e_{34}^{(r_n)}\frac{\partial N_i}{\partial\zeta}\frac{\partial N_j}{\partial\zeta}\Bigg)Jd\xi d\eta d\zeta,$$

$$K_{ij}^{(e)}(4,3)=\int_{-1}^{1}\int_{-1}^{1}\int_{-1}^{1}\Bigg(e_{15}^{(r_n)}\frac{\partial N_i}{\partial\xi}\frac{\partial N_j}{\partial\xi}+e_{14}^{(r_n)}\frac{\partial N_i}{\partial\eta}\frac{\partial N_j}{\partial\xi}+e_{13}^{(r_n)}\frac{\partial N_i}{\partial\zeta}\frac{\partial N_j}{\partial\xi}$$
$$+e_{25}^{(r_n)}\frac{\partial N_i}{\partial\xi}\frac{\partial N_j}{\partial\eta}+e_{24}^{(r_n)}\frac{\partial N_i}{\partial\eta}\frac{\partial N_j}{\partial\eta}+e_{23}^{(r_n)}\frac{\partial N_i}{\partial\zeta}\frac{\partial N_j}{\partial\eta}$$
$$+e_{35}^{(r_n)}\frac{\partial N_i}{\partial\xi}\frac{\partial N_j}{\partial\zeta}+e_{34}^{(r_n)}\frac{\partial N_i}{\partial\eta}\frac{\partial N_j}{\partial\zeta}+e_{33}^{(r_n)}\frac{\partial N_i}{\partial\zeta}\frac{\partial N_j}{\partial\zeta}\Bigg)Jd\xi d\eta d\zeta,$$

$$K_{ij}^{(e)}(4,4)=-\int_{-1}^{1}\int_{-1}^{1}\int_{-1}^{1}\Bigg(\varepsilon_{11}^{(r_n)}\frac{\partial N_i}{\partial\xi}\frac{\partial N_j}{\partial\xi}+\varepsilon_{12}^{(r_n)}\frac{\partial N_i}{\partial\xi}\frac{\partial N_j}{\partial\eta}+\varepsilon_{21}^{(r_n)}\frac{\partial N_i}{\partial\eta}\frac{\partial N_j}{\partial\xi}$$
$$+\varepsilon_{13}^{(r_n)}\frac{\partial N_i}{\partial\xi}\frac{\partial N_j}{\partial\zeta}+\varepsilon_{31}^{(r_n)}\frac{\partial N_i}{\partial\zeta}\frac{\partial N_j}{\partial\xi}+\varepsilon_{22}^{(r_n)}\frac{\partial N_i}{\partial\eta}\frac{\partial N_j}{\partial\eta}$$
$$+\varepsilon_{23}^{(r_n)}\frac{\partial N_i}{\partial\eta}\frac{\partial N_j}{\partial\zeta}+\varepsilon_{32}^{(r_n)}\frac{\partial N_i}{\partial\zeta}\frac{\partial N_j}{\partial\eta}+\varepsilon_{33}^{(r_n)}\frac{\partial N_i}{\partial\zeta}\frac{\partial N_j}{\partial\zeta}\Bigg)Jd\xi d\eta d\zeta,$$

where

$$J=\begin{vmatrix}\frac{\partial x_1}{\partial\xi} & \frac{\partial x_1}{\partial\eta} & \frac{\partial x_1}{\partial\zeta}\\ \frac{\partial x_2}{\partial\xi} & \frac{\partial x_2}{\partial\eta} & \frac{\partial x_2}{\partial\zeta}\\ \frac{\partial x_3}{\partial\xi} & \frac{\partial x_3}{\partial\eta} & \frac{\partial x_3}{\partial\zeta}\end{vmatrix}=\frac{(\mathrm{x}_{1,i+1}-\mathrm{x}_{1,i})(\mathrm{x}_{2,i+1}-\mathrm{x}_{2,i})(\mathrm{x}_{3,i+1}-\mathrm{x}_{3,i})}{8}$$